Editors' Suggestion

Electron Scattering in Liquid Water and Amorphous Ice: A Striking Resemblance

Ruth Signorell*
Department of Chemistry and Applied Biosciences, ETH Zürich, Vladimir-Prelog-Weg 2, CH-8093 Zürich, Switzerland

(Received 14 February 2020; accepted 29 April 2020; published 19 May 2020)

The lack of accurate low-energy electron scattering cross sections for liquid water is a substantial source of uncertainty in the modeling of radiation chemistry and biology. The use of existing amorphous ice scattering cross sections for the lack of liquid data has been discussed controversially for decades. Here, we compare experimental photoemission data of liquid water with corresponding predictions using amorphous ice cross sections, with the aim of resolving the debate regarding the difference of electron scattering in liquid water and amorphous ice. We find very similar scattering properties in the liquid and the ice for electron kinetic energies up to a few hundred electron volts. The scattering cross sections recommended here for liquid water are an extension of the amorphous ice cross sections. Within the framework of currently available experimental data, our work answers one of the most debated questions regarding electron scattering in liquid water.

DOI: 10.1103/PhysRevLett.124.205501

Low-energy electron scattering in liquid water is recognized as having important implications in a wide range of fields, including radiation damage in aqueous systems [1–9]. These electrons are abundantly produced during slowing-down processes from various precursor processes. The quantitative description of the transport properties of sub-keV electrons in liquid water, however, has been very challenging due to the lack of reliable electron scattering cross sections (CSs) for the liquid and related quantities, such as electron inelastic and elastic mean free paths (referred to as IMFPs and EMPFs, respectively).

Various models have been proposed for the prediction of mean free paths (MFPs), many of which are based on different treatments of the dielectric response (see, e.g., [5,10–16], and references therein). It has been shown that predicted MFPs are very sensitive to the particular model used for electron kinetic energies (eKEs) below a few hundred eV, with the biggest deviations in the range below a few 10 eV, where the appropriateness of some model assumptions are disputed. The situation in the subexcitation range (eKEs ≤ 7 eV) remains particularly uncertain. Model approaches are largely missing in this range due to the complexity of the relevant processes to be described.

The retrieval of CSs from experimental data has been severely hampered by difficulties in performing experiments with low-energy electrons for liquid water. Liquid bulk water is not compatible with the vacuum required for such experiments. Substantial progress has been made in recent years through the invention of liquid water microjet photoelectron spectroscopy [17] and droplet photoelectron imaging [18]. This has resulted in experimental electron attenuation lengths (EALs) [19–21], photoelectron anisotropy parameters [22–24], and liquid CSs in the subexcitation range determined from droplet photoelectron images [18] but not yet in detailed CSs for the liquid that cover the whole sub-keV range. Detailed CSs, i.e., multiple differential CSs and energetics, exist only for amorphous ice retrieved from experimental ice data by Sanche and coworkers for the entire range below 100 eV eKE [25,26]. The use of these ice CSs for the lack of liquid CSs has become one of the most controversially discussed issues in the field, so far with no clear outcome. This controversy mainly resulted from the fact that some experimental observations in the liquid that are indirectly related to scattering CSs could seemingly not be modeled accurately enough with the ice CSs. Differences between theoretically modeled liquid MFPs and those derived from the experimental amorphous ice CSs also contributed to the dispute. *Ad hoc* scaling factors for CSs have been proposed to account for these potential differences between ice and liquid (see, e.g., [5,6,12,27,28], and references therein). Even though firm physical arguments in favor of rather than against a close resemblance of liquid and ice CSs have been put forward (e.g., Refs. [25,26]), a confirmation based on a quantitative assessment of experimental data has not been attempted so far. In this work, we combine the most reliable experimental information available from photoelectron spectroscopy of liquid water microjets and water droplets with detailed electron scattering simulations using ice CSs to resolve this issue. The goal is to provide a recommendation for electron scattering CSs for liquid water in the entire sub-keV range.

Experimentally determined effective electron attenuation lengths EAL^{eff} [19], anisotropy parameters β [22–24], and photoelectron velocity map images (VMIs) [18] from liquid water studies are compared with corresponding predictions using the amorphous ice CSs from Refs. [25,26]. The latter were retrieved from electron energy loss spectra recorded for amorphous ice films. The EAL^{eff} and β parameters were

 © 2020 American Physical Society

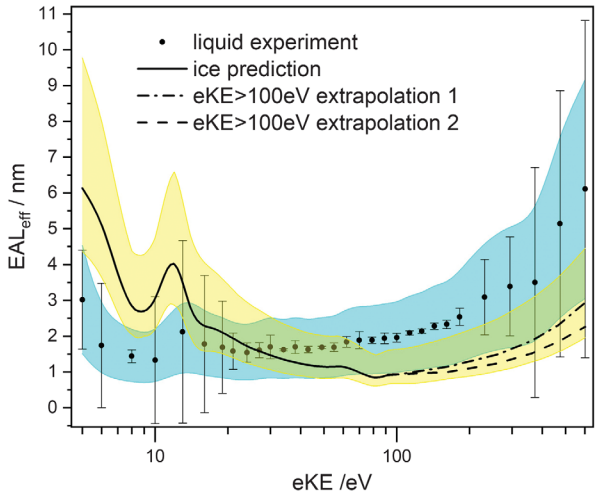

FIG. 1. Effective attenuation length $\mathrm{EAL}^{\mathrm{eff}}$. Experimental effective attenuation length $\mathrm{EAL}_S^{\mathrm{eff}}$ for liquid water from Ref. [19] (black dots). The black error bars for $\mathrm{EAL}_S^{\mathrm{eff}}$ indicate three standard deviations of data resulting from measurements on different days [19], while the blue shaded area represents an estimate of additional systematic uncertainties arising from various sources (Ref. [30], Sec. S1). Both contributions determine the total uncertainty of $\mathrm{EAL}_S^{\mathrm{eff}}$. Monte Carlo prediction of the effective attenuation length $\mathrm{EAL}_M^{\mathrm{eff}}$ using electron scattering CSs derived from experiments on amorphous ice [25,26] (full black line). The CSs above 100 eV eKE (dash-dotted line) are obtained by extrapolation with the model from Ref. [10]. The uncertainty for $\mathrm{EAL}_M^{\mathrm{eff}}$ (shaded yellow area) corresponds to an uncertainty of the absolute total CSs of 45% [25,26]. The dashed line is obtained by extrapolation of the CSs with the model from Ref. [11].

obtained from liquid water microjet measurements, while the VMIs were recorded for water droplets. These liquid measurements were performed at a liquid temperature in the range of ~240–270 K (i.e., mainly for supercooled water). The calculated $\mathrm{EAL}^{\mathrm{eff}}$, β parameters, and VMIs are obtained from a detailed electron scattering model based on a Monte Carlo solution of the transport equation using extended ice CSs (Refs. [18,24–26,29] and Ref. [30], Secs. S1–S5). The model reproduces the exact experimental conditions of each respective experiment, i.e., relevant experimental arrangements, intensity distribution of the ionizing radiation in the liquid samples, and electron sampling conditions.

Figure 1 compares the experimental effective attenuation length for liquid water from Ref. [19], $\mathrm{EAL}_S^{\mathrm{eff}}$, with a Monte Carlo prediction, $\mathrm{EAL}_M^{\mathrm{eff}}$, using the electron scattering CSs of amorphous ice from Refs. [25,26] for eKEs below 100 eV. The definition of $\mathrm{EAL}^{\mathrm{eff}}$ deviates from the usual definition of an EAL (Ref. [30], Sec. S1). In essence, the pioneering experiments of Ref. [19] amounted to an elegant measurement of the absolute photoemission yield for liquid water, which was converted into an effective $\mathrm{EAL}_S^{\mathrm{eff}}$. In the eKE range covered by the amorphous ice data (eKE < 100 eV), $\mathrm{EAL}_S^{\mathrm{eff}}$ and $\mathrm{EAL}_M^{\mathrm{eff}}$ agree very well within their respective uncertainties—and there is no systematic deviation between the two, e.g., one of them consistently higher than the other. Evidently, electron scattering is quite similar in water and ice, and the amorphous ice CSs from Refs. [25,26] are clearly adequate to predict properties of the liquid. Even though the authors of Ref. [19] emphasize that background instabilities make their results less reliable below eKEs ~10 eV, we show these data in Fig. 1 for completeness. Secondary electrons, phonon scattering, and background effects are major issues in this energy region (Ref. [30], Sec. S1).

Experimental amorphous ice CSs are available only up to 100 eV [25]. For calculations beyond that range, we therefore have to follow a different line in order to compare with the $\mathrm{EAL}_S^{\mathrm{eff}}$ of Ref. [19] up to ~600 eV. Given the large total uncertainties of the $\mathrm{EAL}_S^{\mathrm{eff}}$ data for eKE > 100 eV (Fig. 1), nothing would be gained by extracting liquid CSs from a fit to the $\mathrm{EAL}_S^{\mathrm{eff}}$. Instead, we suggest the approach described in Ref. [30], Sec. S5, to extrapolate liquid CSs for eKE above 100 eV in order to predict $\mathrm{EAL}^{\mathrm{eff}}$ in that range. The approach uses the model for liquid water of Ref. [10]—taking only the energy dependence of the electronically inelastic mean free path rather than its absolute values—to extrapolate the differential CSs for amorphous ice at 100 eV from Ref. [25] to higher eKE values. Figure 1 compares the $\mathrm{EAL}_M^{\mathrm{eff}}$ (dash-dotted line) thus predicted with the $\mathrm{EAL}_S^{\mathrm{eff}}$ from Ref. [19]. Within uncertainties, the extrapolation yields a similarly good agreement between the two $\mathrm{EAL}^{\mathrm{eff}}$ datasets above 100 eV, as was obtained with the amorphous ice data for eKEs below 100 eV. The model of Ref. [10] is based on calculations of the IMFP from the optical energy-loss function using the relativistic full Penn algorithm. The theoretically predicted absolute values were scaled by factor of ~3.1 to match the (lower) electron loss CSs at 100 eV of Ref. [25]. This scaling factor reduces to ~1.8 if the model from Ref. [11] (dashed line, Fig. 1) is used instead of Ref. [10]. The reduction originates from the inclusion of exchange and correlation effects in the former model in Ref. [11].

The photoelectron anisotropy parameters β_T and β_N recorded for liquid water in Refs. [22,23] provide a second experimental dataset for the comparison of electron scattering in liquid water and amorphous ice for eKEs above 10 eV. The results are illustrated in Fig. 2(a) for ionization from the $O1s$ orbital and in Fig. 2(b) for ionization from the valence orbitals. The predictions β_M based on the amorphous ice CSs from Refs. [25,26] are described in Ref. [30], Sec. S2. For the calculated β_M above eKEs of 100 eV, we use the same extrapolation as described above for $\mathrm{EAL}_M^{\mathrm{eff}}$ with the model from Ref. [10]. The very good agreement between liquid water and ice β parameters (within the uncertainties indicated in Fig. 2) confirms the similarity of electron scattering in the two phases already found in Fig. 1 for $\mathrm{EAL}^{\mathrm{eff}}$. Again, no meaningful improvement of

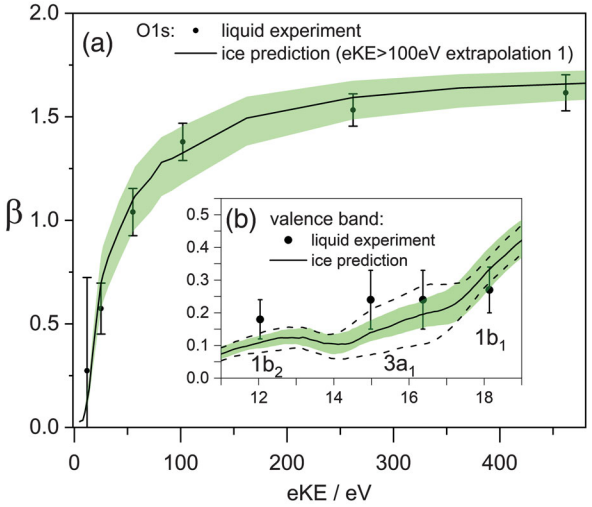

FIG. 2. Anisotropy parameters $\boldsymbol{\beta}$. (a) Experimental β_T for ionization from the $O1s$ orbital of liquid water from Ref. [22] (black dots). Monte Carlo prediction β_M for ionization from $O1s$ using electron scattering cross sections derived from experiments on amorphous ice [25,26] (full black line). The black error bars for β_T indicate three standard deviations quoted in Ref. [22]. The uncertainty for β_M (shaded green area) corresponds to an uncertainty of 20% in the relative cross sections for electronically inelastic and quasielastic scattering [25,26]. (b) Experimental β_N for ionization from the three valence orbitals $1b_1$, $3a_1$, and $1b_2$ of liquid water from Ref. [23] (black dots). Monte Carlo prediction β_M for ionization from the valence orbitals using electron scattering cross sections derived from experiments on amorphous ice [25,26] and water cluster data [24] (full black line). The black error bars for β_N indicate the statistical errors quoted in Ref. [23]. The uncertainty for β_M (shaded green area) is the same as in (a). The dashed lines represent uncertainties arising from the uncertainty of the hexamer water cluster [24].

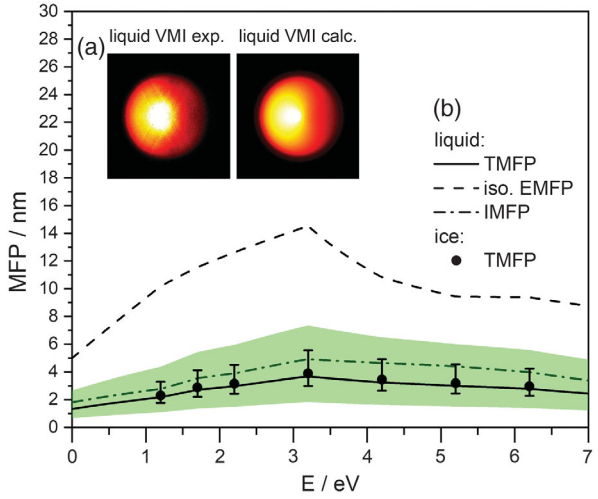

FIG. 3. MFPs for subexcitation electrons. (a) VMI photoelectron spectra of water droplets recorded at a photon energy of 14.9 eV (see also [18,36]). Left: Experimental spectrum. Right: Spectrum simulated with liquid CSs (Ref. [30], Sec. S5). (b) TMFP of amorphous ice (black dots) with uncertainties (black error bars) from Refs. [25,26] and of liquid water (black full line) with uncertainties (green shaded area) (Ref. [30], Sec. S3). Total IMFP (black dash-dotted line) and isotropic EMFP (black dashed line) of liquid water. The total IMPF includes all inelastic channels (electronic, vibrational, and phonon). E is the electron's total energy with respect to the vacuum level [25,26].

the CSs could be gained from fitting to the experimental β parameters.

Reliable information on subexcitation electron scattering became recently available from VMI photoelectron studies of droplets after EUV excitation at more than 40 different photon energies below ~15.4 eV [18,29]. The droplet VMIs [Fig. 3(a)] contain information on the eKE and entire photoelectron angular distribution, which goes beyond that of a single β parameter. The cross sections for liquid water were directly extracted from fits of calculated droplet VMIs to experimental VMIs as described in Refs. [18,29]. It turned out that the experimental droplet VMIs were best reproduced by the simulations when fixing the liquid CSs at the supporting points to those of amorphous ice [25] without further refinement, indicating that the liquid water and the amorphous ice cross sections are very similar in the subexcitation regime. As explained in Ref. [30], Secs. S3 and S5, we have slightly refined the previous liquid CSs [18,29] using the entire information for ice in Refs. [25,26]. We determine somewhat higher uncertainties for the absolute values of the liquid CSs (~factor of 2) compared with ice CSs in the subexcitation regime (30%). The close agreement between liquid and ice is visualized in Fig. 3(b) for the total MFP (TMFP), i.e., the combined MFP of all inelastic and isotropic elastic (momentum transfer CS, transport CS) contributions. The liquid water TMFPs (full black line) have larger uncertainties (shaded green area) compared with amorphous ice (black dots with error bars). The total IMPF (dash-dotted line) and the isotropic EMPF (dashed line) of liquid water are also indicated in Fig. 3(b). Further confirmation of the close similarity between liquid and ice CSs is provided by the good agreement between thermalization lengths measured in the liquid [35] with predictions using the amorphous ice CSs [12,28] for eKEs below ~4 eV. *Ad hoc* upscaling ice CSs by a factor of 2, as suggested in Refs. [12,27,28] to better represent liquid CSs, in fact deteriorated the agreement with the experimental thermalization lengths in Ref. [12].

Currently known observables (EAL^{eff}, β, and VMI) characteristic of the scattering behavior of electrons in liquid water below eKEs of 100 eV can be predicted with CSs for amorphous ice within the quoted uncertainties (Figs. 1–3). Above 100 eV, the scattering behavior of electrons is similarly well predicted by the suggested extrapolation of the amorphous ice CSs on the basis of the functional form of the energy dependence predicted theoretically for liquid water [10]. All of these results taken together lead to the expectation that the electron scattering cross sections in liquid water and ice agree at least within a factor of 2.

Currently available experimental data for the liquid are not sufficiently accurate to bracket this even more narrowly. Fitting the CSs for the liquid to current experimental data (Figs. 1 and 2) would not offer any improvement over using the recommended liquid CSs described in Ref. [30], Sec. S5. The agreement between experimental liquid and ice data reported here is generally closer than the one between experimental and theoretical liquid data. Based on the following general physical considerations, already outlined in Refs. [25,26], one might in fact expect an even closer agreement between liquid and ice CSs than current uncertainties suggest. The major differences between electron scattering in the gas phase (isolated molecules) and in the condensed phase arise from the change in the density of the scattering centers and from the intermolecular interactions. Short-range interactions (mainly hydrogen bonds) give rise to low-energy phonons (hindered rotations and translations), while long-range effects—mainly through dielectric screening—directly correlate with the density. Intermolecular interactions are relatively weak (on the order of 0.1 eV or less) and mostly affect the phonon spectrum (and thus phonon scattering). These interactions are too weak (percent of electronic energies) to affect the electronic structure significantly. Apart from these energetic effects (the interaction strength with a scattering center), electron scattering in the condensed phase is also influenced by the interference between neighboring scattering events, a direct consequence of the increased density. It is important to note that such interferences are naturally contained in experimental CSs and, hence, also in the effective CSs reported here (see also [25,26]). As the density and the degree of disorder are very similar in liquid water and amorphous ice, the same should hold for interaction strengths, screening, and interference behavior. Consequently, one expects very similar CSs in the liquid and the amorphous ice. The only remaining effect that could cause a difference between scattering in water and ice is the difference in temperature. The effect would potentially be most pronounced in the subexcitation regime, where phonons are important. At higher temperatures, thermally populated excited phonon levels could cause an increase of eKE in a scattering event. On average, this could reduce the energy loss per scattering event for the low-energy phonon channels in the liquid. At the thermal energies of the liquids considered here (on the order of 0.01 eV), this effect is not expected to be very pronounced. This is also in agreement with the fact that there is actually no evidence for larger differences between ice and liquid in the subexcitation range (Fig. 3). Finally, our results exclude proposed *ad hoc* scaling factors of more than 2 between ice and liquid CSs, for both inelastic and isotropic (transport) elastic CSs, and they also provide evidence against the use of smaller scaling factors (Ref. [30], Sec. S5).

The present work resolves the controversy regarding the difference in scattering behavior of electrons in liquid water and amorphous ice, based on experimental data for liquid and ice. The close similarity of electron scattering in the liquid and in ice finally allows one to bracket the range of scattering cross sections for the liquid. Compelling evidence is provided that the previously available ice cross sections from Sanche and co-workers [25,26] with the extensions described in the present work currently provide the most reliable cross sections for the liquid (Ref. [30], Sec. S5, Table S1), with maximum uncertainties on the order of a factor of 2. *Ad hoc* scaling of the ice cross sections as previously suggested is clearly not recommended. The present results are expected to have far-reaching implications for the modeling of electron scattering in aqueous environments and, thus, for the understanding of chemical and cellular radiation damage.

This project has received funding from the European Union's Horizon 2020 research and innovation program from the European Research Council under the Grant Agreement No. 786636, and the research was supported by the NCCR MUST, funded by the Swiss National Science Foundation (SNSF), through ETH-FAST, and through SNSF Project No. 200020_172472. The author thanks all co-workers and collaborators who have contributed to the previous experimental and theoretical work that is discussed in the current publication. The author is also a grateful recipient of a Humboldt Research Prize form the Alexander von Humboldt Foundation and a Mildred Dresselhaus Guestprofessorship from the Centre for Ultrafast Imaging in Hamburg.

*Corresponding author.
rsignorell@ethz.ch

[1] B. C. Garrett *et al.*, Chem. Rev. **105**, 355 (2005).
[2] E. Alizadeh and L. Sanche, Chem. Rev. **112**, 5578 (2012).
[3] E. Alizadeh, T. M. Orlando, and L. Sanche, Annu. Rev. Phys. Chem. **66**, 379 (2015).
[4] B. Abel, Annu. Rev. Phys. Chem. **64**, 533 (2013).
[5] H. Nikjoo, D. Emfietzoglou, T. Liamsuwan, R. Taleei, D. Liljequist, and S. Uehara, Rep. Prog. Phys. **79**, 116601 (2016).
[6] V. Lemelin and L. Sanche, in *Radiation in Bioanalysis: Spectroscopic Techniques and Theoretical Methods*, edited by A. S. Pereira, P. Tavares, and P. Limão-Vieira (Springer International Publishing, Cham, 2019), p. 3.
[7] B. Boudaiffa, P. Cloutier, D. Hunting, M. A. Huels, and L. Sanche, Science **287**, 1658 (2000).
[8] J. M. Herbert and M. P. Coons, Annu. Rev. Phys. Chem. **68**, 447 (2017).
[9] R. M. Young and D. M. Neumark, Chem. Rev. **112**, 5553 (2012).
[10] H. Shinotsuka, B. Da, S. Tanuma, H. Yoshikawa, C. J. Powell, and D. R. Penn, Surf. Interface Anal. **49**, 238 (2017).
[11] D. Emfietzoglou, I. Kyriakou, R. Garcia-Molina, and I. Abril, Surf. Interface Anal. **49**, 4 (2017).
[12] J. Meesungnoen, J. P. Jay-Gerin, A. Filali-Mouhim, and S. Mankhetkorn, Radiat. Res. **158**, 657 (2002).

[13] D. Emfietzoglou and H. Nikjoo, Radiat. Res. **163**, 98 (2005).
[14] M. Dingfelder, D. Hantke, M. Inokuti, and H. G. Paretzke, Radiat. Phys. Chem. **53**, 1 (1998).
[15] A. Akkerman and E. Akkerman, J. Appl. Phys. **86**, 5809 (1999).
[16] J. C. Ashley, J. Electron Spectrosc. Relat. Phenom. **46**, 199 (1988).
[17] B. Winter, R. Weber, W. Widdra, M. Dittmar, M. Faubel, and I. V. Hertel, J. Phys. Chem. A **108**, 2625 (2004).
[18] R. Signorell, M. Goldmann, B. L. Yoder, A. Bodi, E. Chasovskikh, L. Lang, and D. Luckhaus, Chem. Phys. Lett. **658**, 1 (2016).
[19] Y.-I. Suzuki, K. Nishizawa, N. Kurahashi, and T. Suzuki, Phys. Rev. E **90**, 010302(R) (2014).
[20] N. Ottosson, M. Faubel, S. E. Bradforth, P. Jungwirth, and B. Winter, J. Electron Spectrosc. Relat. Phenom. **177**, 60 (2010).
[21] F. Buchner, T. Schultz, and A. Lübcke, Phys. Chem. Chem. Phys. **14**, 5837 (2012).
[22] S. Thürmer, R. Seidel, M. Faubel, W. Eberhardt, J. C. Hemminger, S. E. Bradforth, and B. Winter, Phys. Rev. Lett. **111**, 173005 (2013).
[23] J. Nishitani, C. W. West, and T. Suzuki, Struct. Dyn. **4**, 044014 (2017).
[24] S. Hartweg, B. L. Yoder, G. A. Garcia, L. Nahon, and R. Signorell, Phys. Rev. Lett. **118**, 103402 (2017).
[25] M. Michaud, A. Wen, and L. Sanche, Radiat. Res. **159**, 3 (2003).
[26] M. Michaud and L. Sanche, Phys. Rev. A **36**, 4672 (1987).
[27] V. Cobut, Y. Frongillo, J. P. Patau, T. Goulet, M. J. Fraser, and J. P. Jay-Gerin, Radiat. Phys. Chem. **51**, 229 (1998).
[28] S. Uehara and H. Nikjoo, J. Radiat. Res. **47**, 69 (2006).
[29] D. Luckhaus, Y.-I. Yamamoto, T. Suzuki, and R. Signorell, Sci. Adv. **3**, e1603224 (2017).
[30] See Supplemental Material at http://link.aps.org/supplemental/10.1103/PhysRevLett.124.205501 for experimental and modeling details, and the electron scattering cross sections for liquid water (Sec. S5), which includes Refs. [31–34].
[31] L. Ban, T. E. Gartmann, B. L. Yoder, and R. Signorell, Phys. Rev. Lett. **124**, 013402 (2020).
[32] S. Amanatidis, B. L. Yoder, and R. Signorell, J. Chem. Phys. **146**, 224204 (2017).
[33] B. L. Yoder, A. H. C. West, B. Schläppi, E. Chasovskikh, and R. Signorell, J. Chem. Phys. **138**, 044202 (2013).
[34] Y. Itikawa and N. Mason, J. Phys. Chem. Ref. Data **34**, 1 (2005).
[35] V. V. Konovalov, A. M. Raitsimring, and Y. D. Tsvetkov, Radiat. Phys. Chem. **32**, 623 (1988).
[36] L. Ban, B. L. Yoder, and R. Signorell, Annu. Rev. Phys. Chem. **71**, 315 (2020).